Supporting Information

Bioadhesive Polydopamine-Vitamin A Derivative Hydrogels Reprogram the Wound Microenvironment for Scarless Wound Healing and Hair Follicle Regeneration

Kang Wang[a]‡, Hengjie Zhang[b],‡, Mengxin Wang[b], Zhengyong Li[a], Wu Wu[a], Pengcheng Liu[a], Ruiqi Liu[a], Zhipeng Gu[b], Yiwen Li[b*], Zhenyu Zhang[a*]

a. Department of Plastic and Burn Surgery, West China Hospital, West China School of Medicine, Sichuan University, Chengdu 610041, China.

b. College of Polymer Science and Engineering, State Key Laboratory of Advanced Polymer Materials, Sichuan University, Chengdu 610065, China.

‡: These authors contributed equally to this work.

Email: zhangzhenyu@scu.edu.cn (Z.Z.)； ywli@scu.edu.cn (Y.L.)

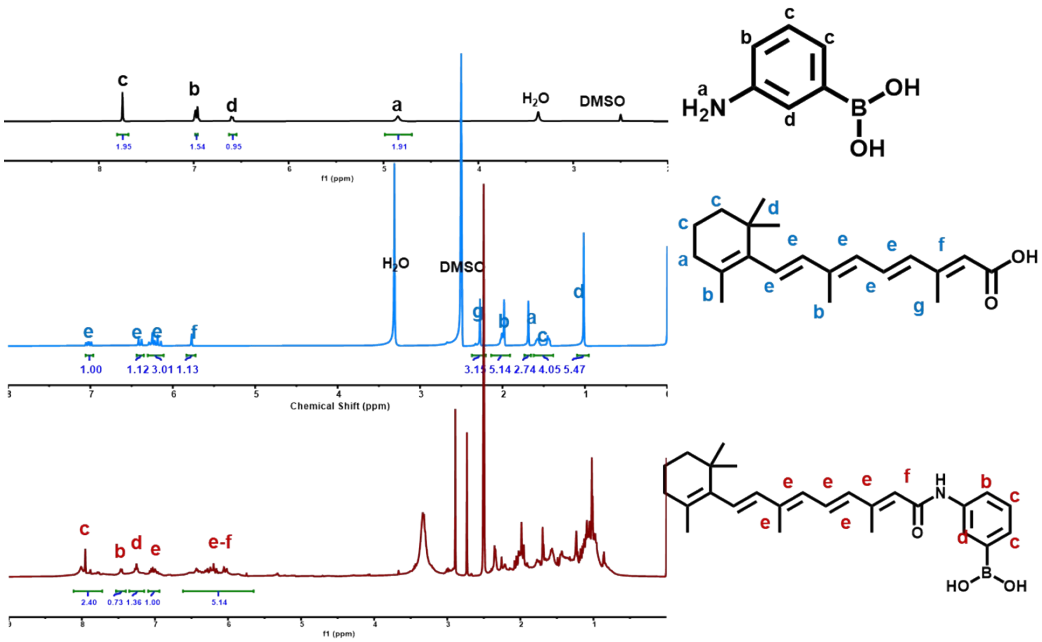

Figure S1. [1]H NMR spectra and chemical structures of 3-ABA, RA-COOH, and RA-BOH.

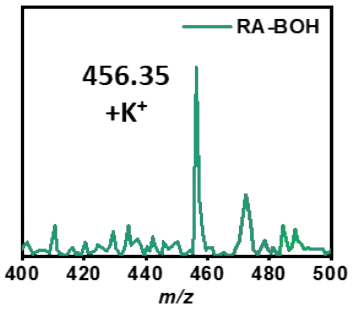

Figure S2. Molecular weight and mass spectrum of RA-BOH.

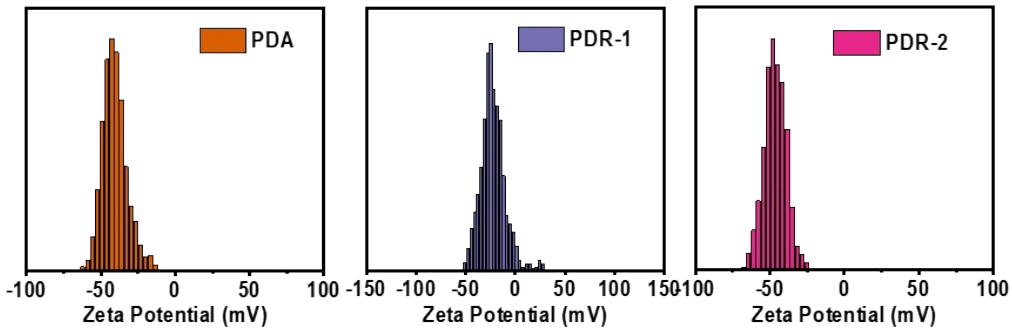

Figure S3. Zeta potential measurements of PDA NPs, PDR-1 NPs, and PDR-2 NPs.

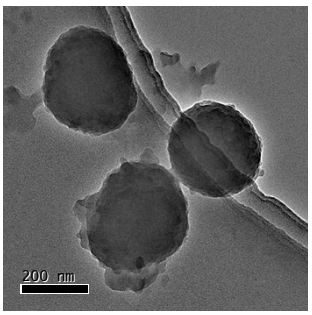

Figure S4. TEM images of PDR-1 NPs.

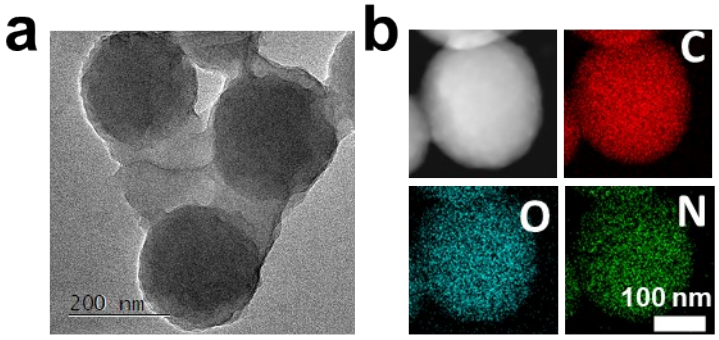

Figure S5. (a) TEM images and (b) elemental analysis of PDR-2 NPs.

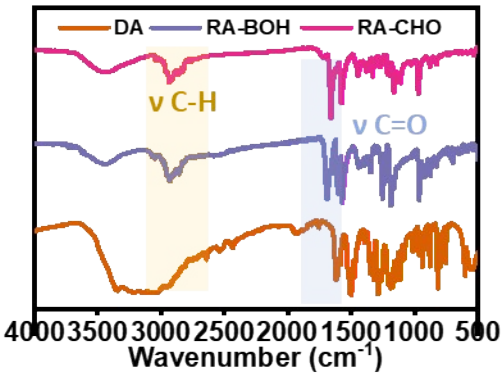

Figure S6. FTIR spectra of DA, RA-BOH, and RA-CHO.

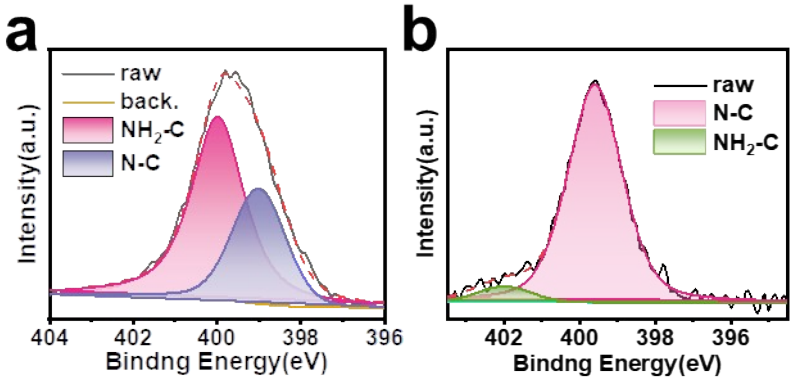

Figure S7. N1s XPS spectra of (a) PDA NPs and (b) PDR-1 NPs.

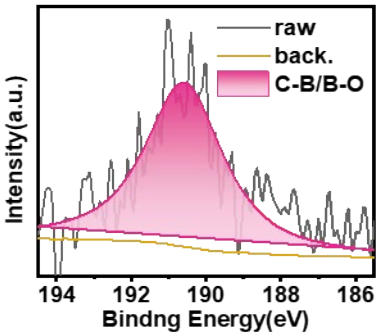

Figure S8. B1s XPS spectrum of PDR-1 NPs.

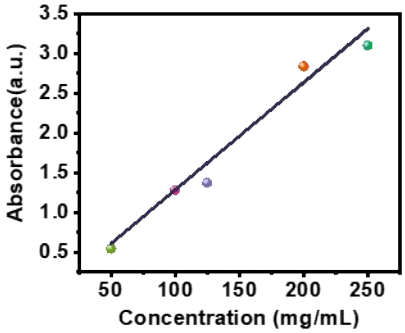

Figure S9. Drug release standard curve of RA-CHO.

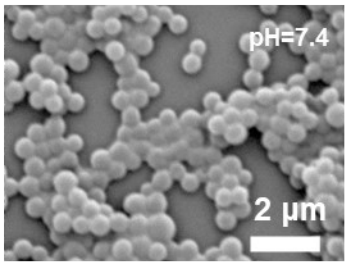

Figure S10. SEM image of PDR-2 NPs after 24 h in a PBS buffer (pH =7.4).

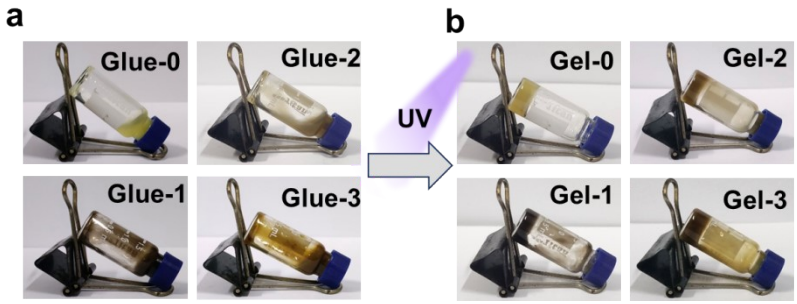

Figure S11. Optical images of the bio-glues undergoing UV irradiation to form hydrogels.

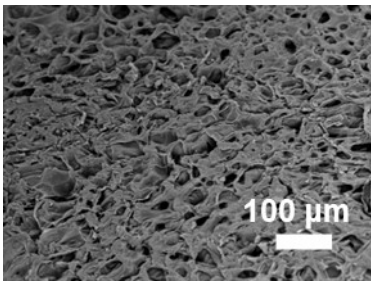

Figure S12. SEM image of Gel-0.

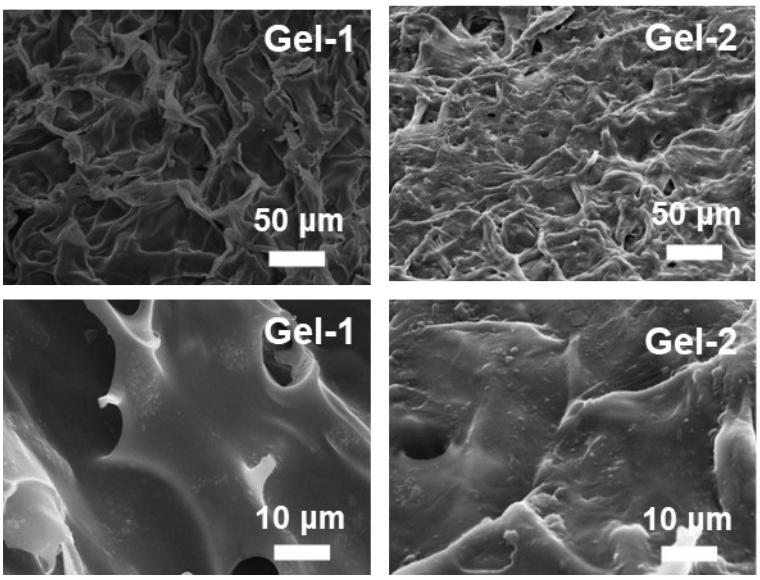

Figure S13. SEM images of Gel-1and Gel-2.

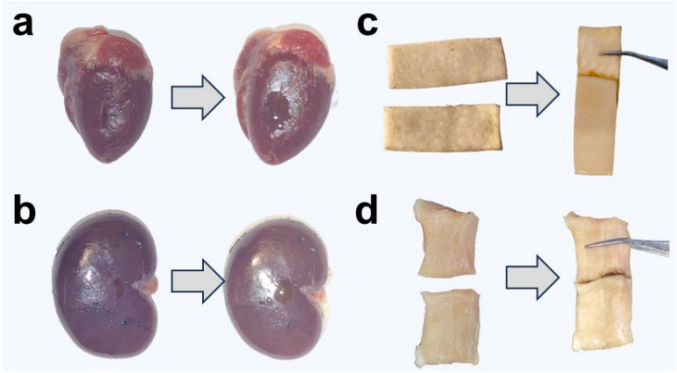

Figure S14. Tissue adhesion performances of Gel-3: (a) heart, (b) liver, (c) porcine skin, and (d)muscle.

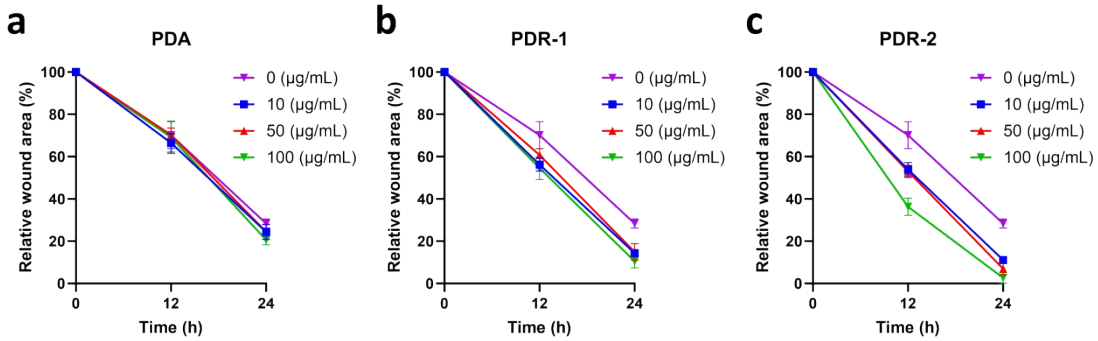

Figure S15. Quantitative analysis of cell migration rates in scratch assays under PDA, PDR-1, and PDR-2 nanoparticle concentrations.

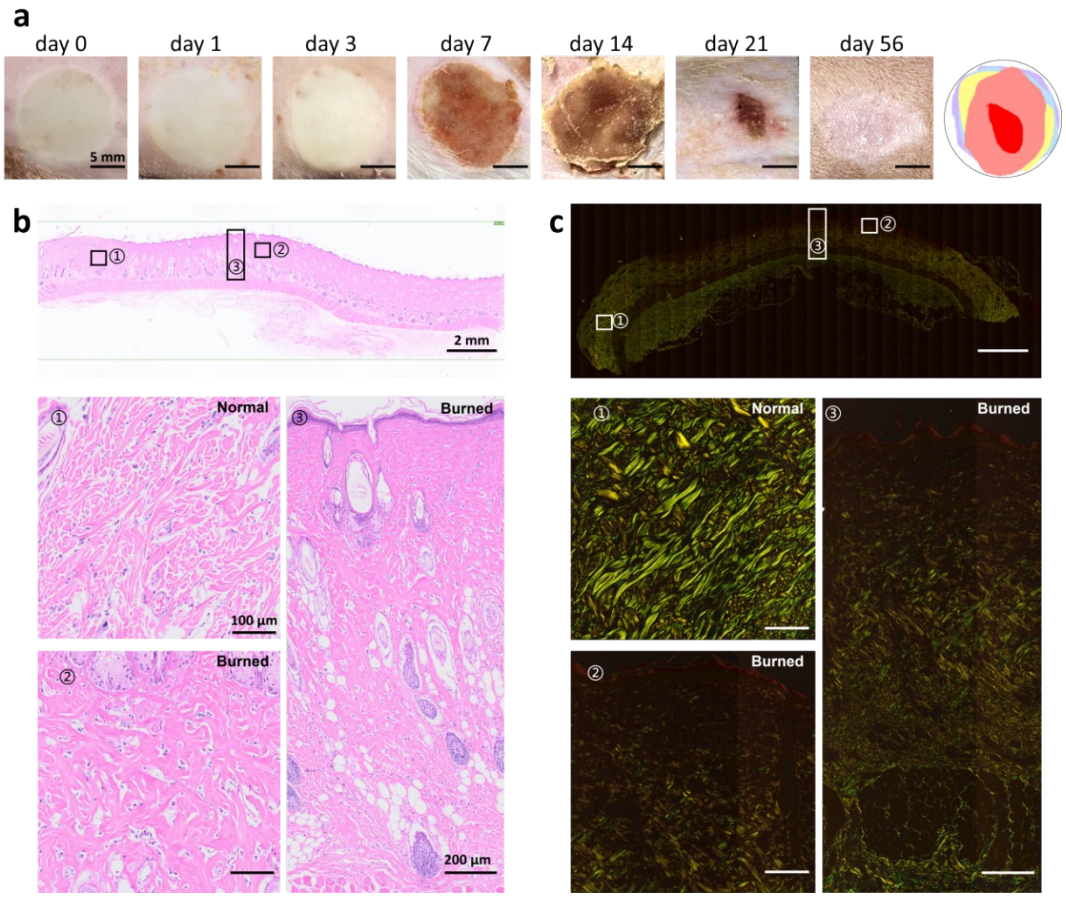

Figure S16. Evaluation of deep second-degree burn model in rats. (a) Macroscopic observation of the wound appearance. (b, c) Representative H&E and Sirius red staining images of tissue sections obtained 1 hour post-injury, cut through the center of the burn wound.

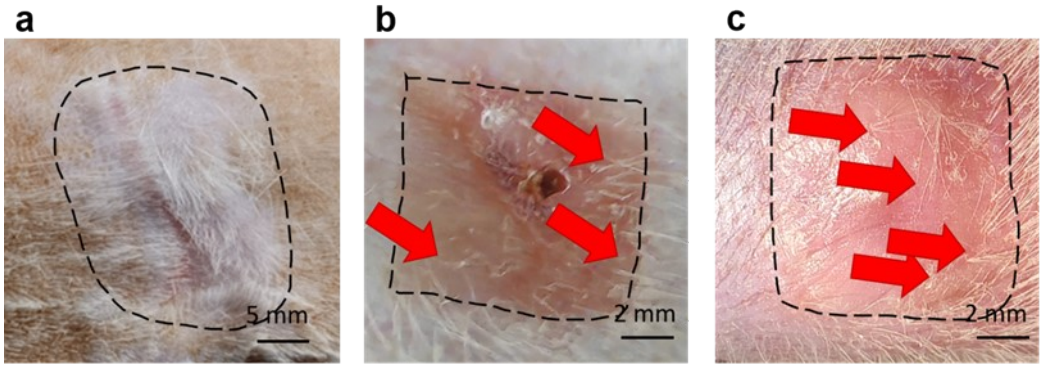

Figure S17. Gross Observation of Hair Follicle Regeneration Promoted by Gel-3. (a) Macroscopic view of the dorsal burn wound in rats at day 56 post-treatment with Gel-3. The dashed outline indicates the original wound area. (b, c) Gross appearance of

wound sites in the rabbit ear hypertrophic scar model at 21 day and 47 day after Gel-3 treatment. Dashed outlines denote the original wound boundaries, and red arrows

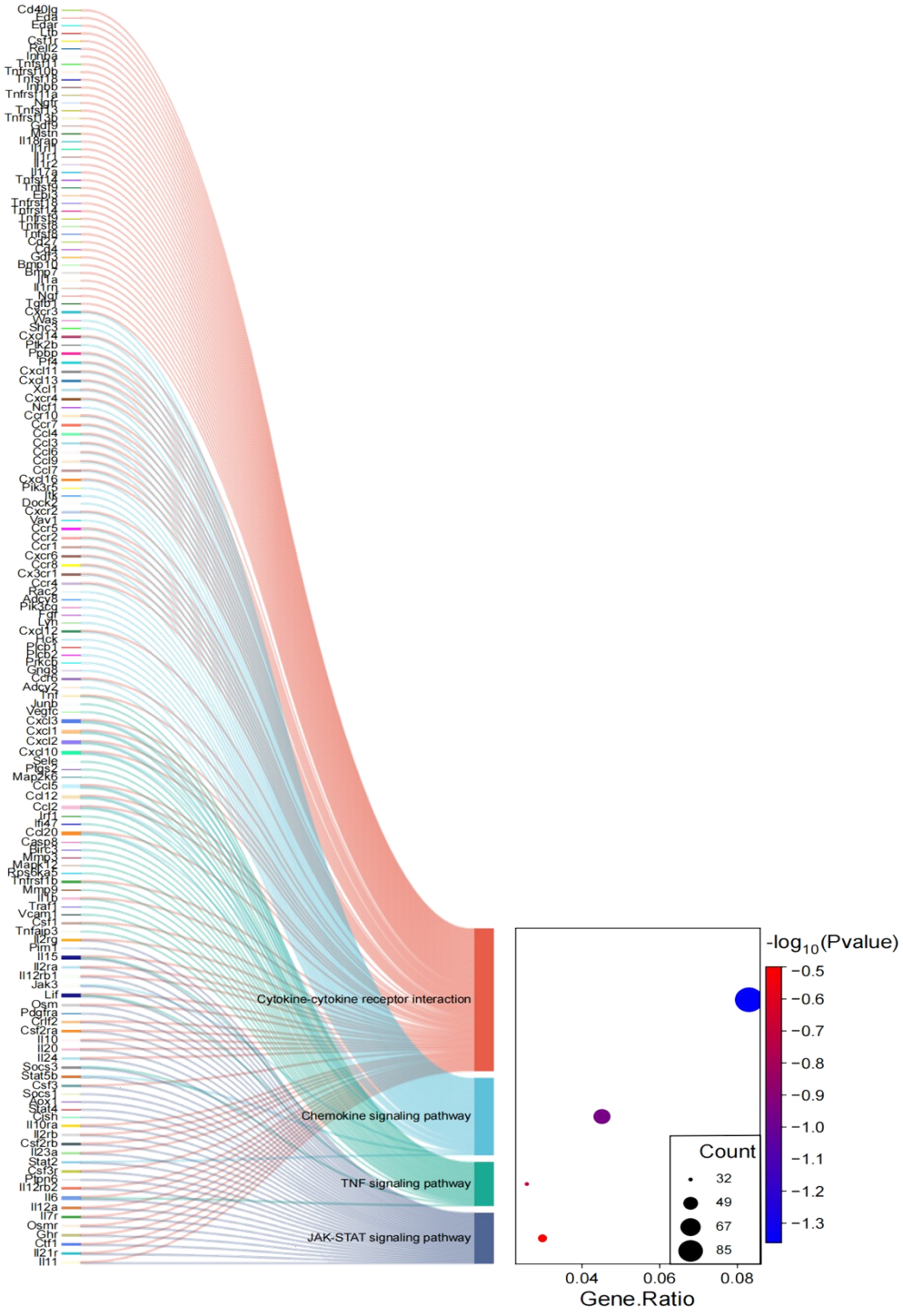

highlight newly regenerated hairs.

Figure S18. KEGG pathway enrichment is visualized as a Sankey dot plot comparing

Gel-3 and Control.

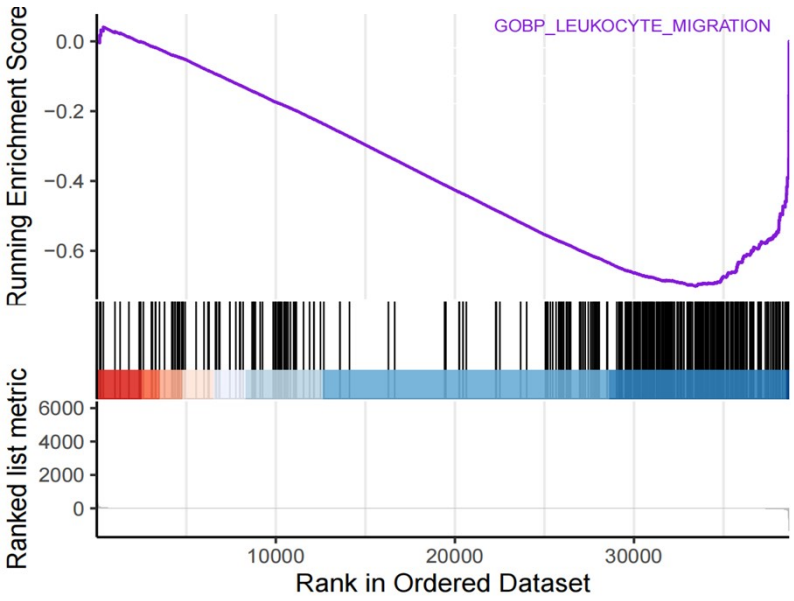

Figure S19. GSEA (GOBP database) analysis of leukocyte migration (Gel-3 VS Control).

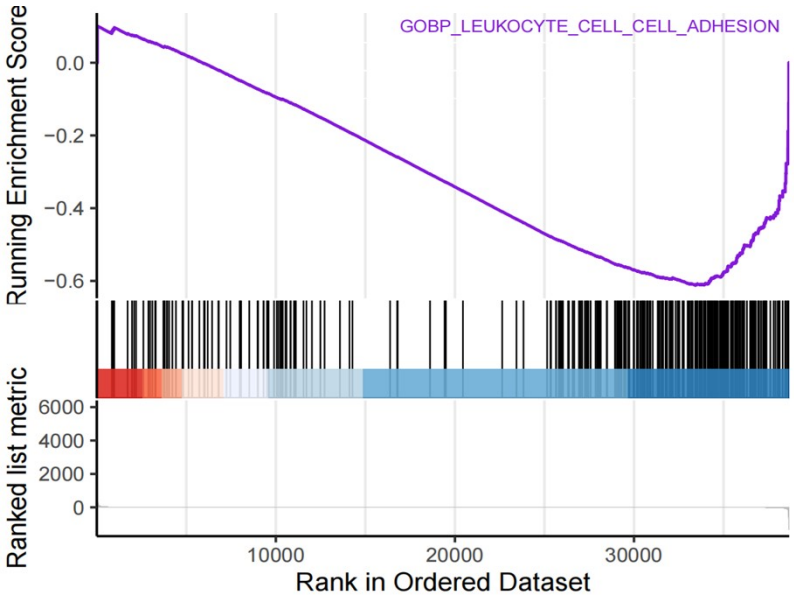

Figure S20. GSEA (GOBP database) analysis of leukocyte cell–cell adhesion (Gel-3 VS Control).

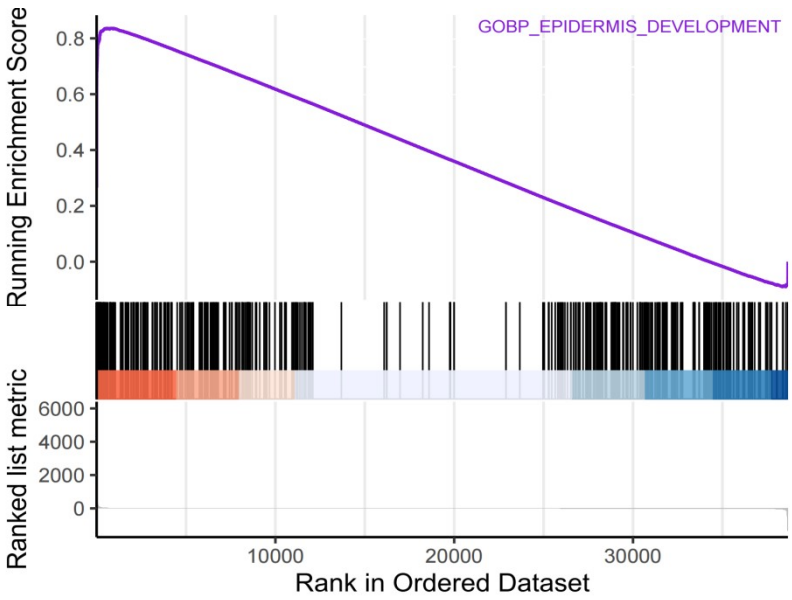

Figure S21. GSEA (GOBP database) analysis of epidermis development (Gel-3 VS Control).

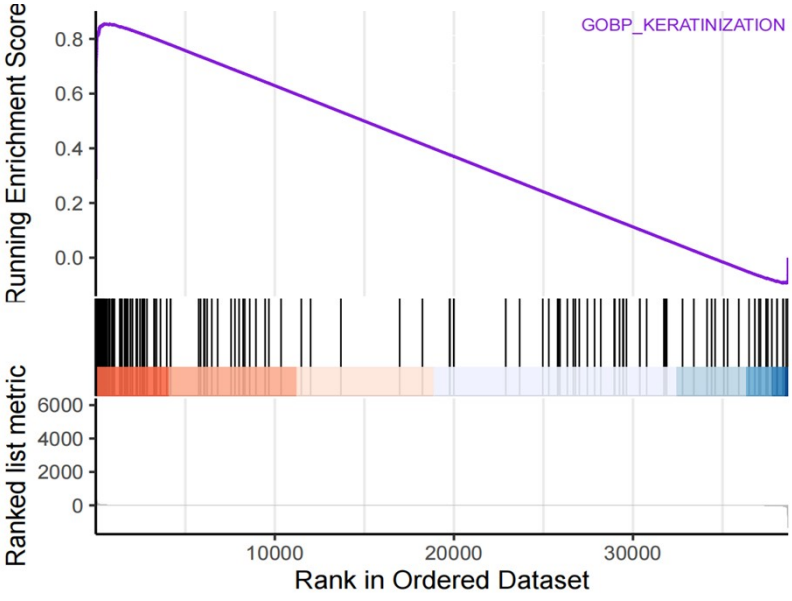

Figure S22. GSEA (GOBP database) analysis of keratinization (Gel-3 VS Control).

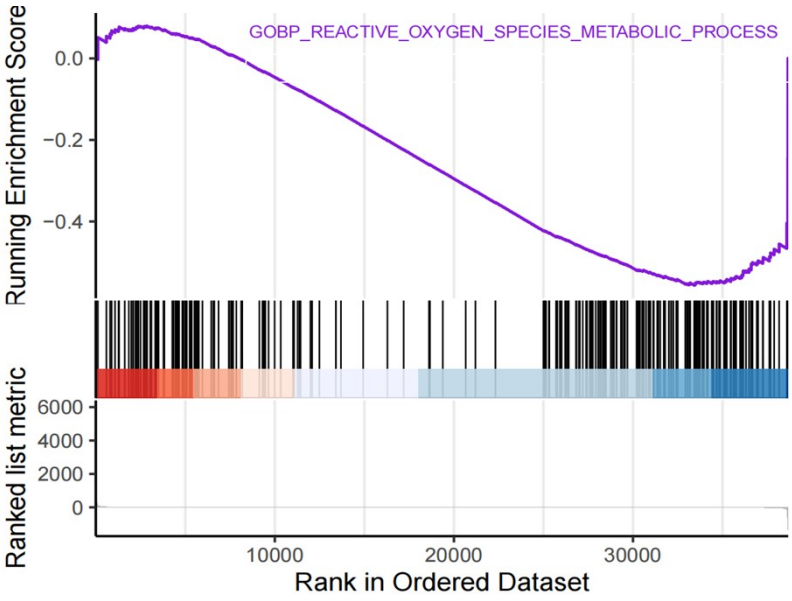

Figure S23. GSEA (GOBP database) analysis of ROS metabolic process (Gel-3 VS Control).